

Review of the extraction of electrochemical kinetic data from electrochemical impedance data using genetic algorithm optimization

D. Macdonald^{1*}, S. Sharifi-Asl¹, G. Engelhardt²

¹Department of Materials Science and Engineering University of California at Berkeley, Berkeley, CA 94720, USA

²OLI Systems, Inc., 240 Cedar Knolls Road, Cedar Knolls, NJ 07927, USA

Received December 26, 2016 Revised January 15, 2016

This present paper was prepared in honor of the contributions of Dr. Zdravko Stoyanov to electrochemical impedance spectroscopy (EIS) on the occasion of his eightieth birthday. Recognizing the seminal contributions that Prof. Stoyanov has made to EIS, in this paper, we illustrate the application of EIS in the analysis of impedance data for passive metal systems; in particular, the impedance of copper in sulfide-containing granitic rock ground water that will exist in the repository for High Level Nuclear Waste (HLNW) in Sweden and Finland. We demonstrate the feasibility of optimizing the Point Defect Model (PDM) upon experimental impedance data to extract values for important model parameters, which in turn can be used to calculate the steady state barrier layer thickness and passive current density as a function of voltage. These quantities are required for determining the corrosion rate of copper in contact with the repository sulfide-containing ground water and hence in estimating canister life-time, which is designed to be of the order of 100,000 years.

Key words: electrochemical impedance spectroscopy, copper, point defect model, optimization.

INTRODUCTION

Professor Zdravko Stoyanov was one of the early pioneers of the modern form of electrochemical impedance spectroscopy (EIS) and has contributed greatly to the rich fabric of this important subject. His many, impressive accomplishments are cataloged in the scientific literature, including this Special Issue commemorating his 80th birthday, and serve as a beacon for those who follow in his footsteps. In this paper, we review how EIS is now used to define the mechanism of the formation of a passive film on a metal surface; in this case, the formation of Cu₂S on Cu in sulfide-containing brine. The present work was performed to provide a scientific basis for estimating the lifetimes of copper canisters in crystalline rock repositories in Sweden that are used for the disposal of high level nuclear waste (HLNW). The paper is presented in honor of the many profound contributions that Professor Zdravko Stoyanov has made to electrochemical impedance spectroscopy.

THEORY

The Point Defect Model was developed over the past thirty-five years by Macdonald and coworkers as a mechanistically-based model that could be tested analytically against experiment [1-3]. The

PDM is now highly developed and, to our knowledge, there are no known conflicts with experiment, where confluence between theory and experiment has been first demonstrated. Indeed, the model has predicted new phenomena that have subsequently been observed, including the photo-inhibition of passivity breakdown (PIPB) [4-7], and has provided a theoretical basis for designing new alloys from first principles [8, 9]. The PDM has been previously used to interpret electrochemical impedance data by optimizing the model on the experimentally-determined real and imaginary components of the interphasial (metal/passive film/solution) impedance, with considerable success [10-14]. An earlier version of the model has been extensively used to analyze data obtained in this laboratory on a program defining the electrochemistry and corrosion behavior of carbon steel in simulated concrete pore water. Our early work [13,15,16], used the commercial DataFit software [16] for optimization, which employs the Levenberg-Marquardt [17] method of minimization, in order to estimate values for various model parameters. The optimization work described in the present paper was performed using the much the same physico-electrochemical model derived from the PDM as in our previous work, with the exception that the model describes a bi-layer film. However, the optimization itself is performed using the newer, more powerful method of optimization; Differential Evolution (DE), using custom software [18]. This algorithm resolves many of the issues

To whom all correspondence should be sent:
E-mail: macdonald@berkeley.edu

associated with parameter optimization of functions of this type, including being less susceptible to being “hung-up” on minima other than the global minimum. Consequently, the quality of solution is vastly improved (several orders of magnitude reduction in the chi-squared error over gradient-based methods). The mechanics of the Evolutionary Algorithm methods are presented in Ref. [19]. Although gradient-based methods are computationally much faster than evolutionary methods, such as DE, without operator experience and the requirement for non-intuitive knowledge

about a highly dimensional system, they are not operationally more efficient. The man-hours saved more than makes up for any shortcomings in terms of computational speed.

THE POINT DEFECT MODEL

As noted above, the PDM was developed to provide an atomic-scale description of the formation and breakdown of passive films [1-5]. The physico-chemical basis of the PDM is shown in Figure 1.

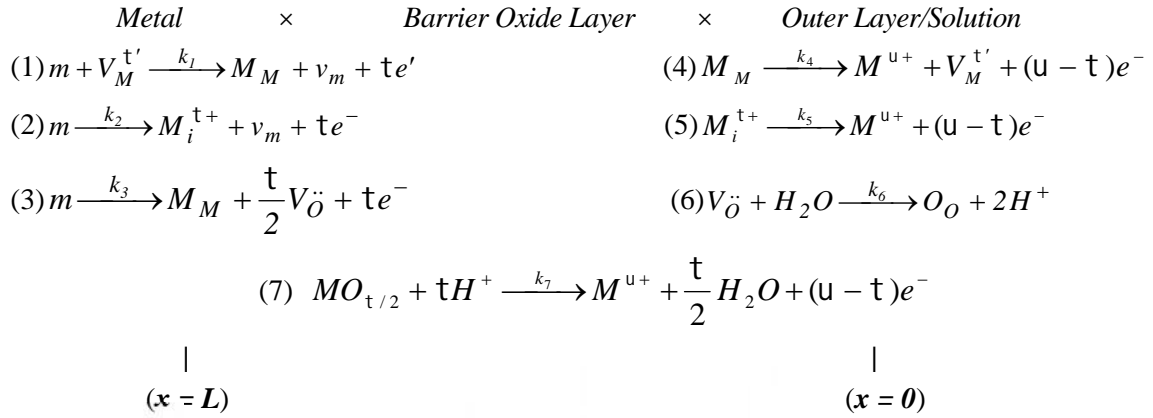


Fig. 1. Interfacial defect generation/annihilation reactions that are postulated to occur in the growth of anodic barrier oxide films according to the Point Defect Model. $m \equiv$ metal atom, $V_M^{X'}$ \equiv cation vacancy on the metal sublattice of the barrier layer, M_i^{X+} \equiv interstitial cation, $M_M \equiv$ metal cation on the metal sublattice of the barrier layer, $V_{\ddot{O}} \equiv$ oxygen vacancy on the oxygen sublattice of the barrier layer, $O_O \equiv$ oxygen anion on the oxygen sublattice of the barrier layer, $M^{\delta+} \equiv$ metal cation in solution.

Briefly, the model postulates that defect generation and annihilation reactions occur at the metal/barrier layer (m/bl) and the barrier layer/outer layer (bl/ol) interfaces, which are separated by a few nano-meters, and that these reactions, as depicted in Figure 1, establish the point defect concentrations within the barrier layer. The charged point defects are envisioned to migrate across the film in a direction that is consistent with their charge and the sign of the electric field. Thus, positively-charged oxygen vacancies and metal interstitials migrate from the m/bl interface, where they are generated by Reactions (2) and (3), respectively, to the bl/s interface, where they are annihilated by Reactions (5) and (6), while negatively-charged cation vacancies migrate in the reverse direction. The electric field strength for oxides is $= 1.5 \times 10^6$ V/cm, but is lower by about an order of magnitude for the more polarizable sulfides. In both cases, the field strength is such that the defects move by migration, not by diffusion. The field strength is postulated to be buffered by Esaki, band-to-band tunneling, possibly via inter band-gap states, and hence is insensitive to the applied voltage and the thickness of the barrier

layer. Finally, it is assumed that the potential drop across the bl/s interface ($\Phi_{f/s}$) is a linear function of the applied voltage and pH

$$\Phi_{f/s} = \alpha V + \beta pH + \Phi_{f/s}^0 \quad (1)$$

such that the potential drop across the m/bl interface is given as

$$\Phi_{m/f} = (1 - \alpha)V - \beta pH - \epsilon L - \Phi_{f/s}^0 \quad (2)$$

where L is the thickness of the barrier layer and $\Phi_{f/s}^0$ is a constant. The form of Equation (1) is dictated by electrical double layer theory for oxide/solution interfaces. Other assumptions and postulates are contained in the original publications [4,5].

The electron current density, I , which is sensed as an electron current in the external circuit, is expressed in terms of the kinetics of all reactions that produce or consume electrons and, hence, is written as:

$$I = F \left\{ \begin{aligned} &\chi k_1 C_v^L + \chi k_2 + \chi k_3 + (\delta - \chi)k_4 \\ &+ (\delta - \chi)k_5 C_i^0 + (\delta - \chi)k_7 \end{aligned} \right\} \quad (3)$$

where C_{ϵ}^L is the concentration of cation vacancies at the m/bl interface and C_i^0 is the concentration of cation interstitials at the bl/ol (bl/s) interface. Note that Equation 3 does not depend upon the concentration of oxygen vacancies or upon the rate constant for Reaction (6), Figure 1. Thus, no relaxations in the impedance response involving oxygen vacancies is predicted, but this is essentially an artifact of considering Reactions (3) and (6), Figure 1, to be irreversible. If this reaction was assumed to be reversible, then a relaxation involving oxygen vacancies would be present. Furthermore, the concentration of H^+ is considered to be constant, corresponding to a well-buffered solution, and is included in the definition of k_7 , as indicated in Equation 6, below. Parenthetically, we note that the inclusion of reversible reactions would allow the PDM to also account for the reduction of passive films, albeit at a considerable cost in mathematical complexity.

Using the method of partial charges, the rate constants for the reactions in the presence of a porous, resistive outer layer are found to be of the form [20]:

Table 1. Coefficients for the rate constants for the reactions that generate and annihilate point defects at the m/bl interface [Reactions (1) – (3)] and at the bl/s interface [Reactions (4) – (6)], Figure 1, and for dissolution of the film [3-5]. $k_i = k_i^0 e^{a_i V} e^{b_i L} e^{c_i pH}$

Reaction	$a_i (V^{-1})$	$b_i (cm^{-1})$	C_i	Units of k_i^o
(1) $m + V_M^{t'} \xrightarrow{k_1} M_M + v_m + te'$	1(1-)	- 1	- 1	$\frac{1}{s}$
(2) $m \xrightarrow{k_2} M_i^{t+} + v_m + te^-$	2(1-)	- 2	- 2	$\frac{mol}{cm^2 s}$
(3) $m \xrightarrow{k_3} M_M + \frac{t}{2} V_{\ddot{O}} + te^-$	3(1-)	- 3	- 3	$\frac{mol}{cm^2 s}$
(4) $M_M \xrightarrow{k_4} M^{u+} + V_M^{t'} + (u - t)e^-$	4		4	$\frac{mol}{cm^2 s}$
(5) $M_i^{t+} \xrightarrow{k_5} M^{u+} + (u - t)e^-$	5		5	$\frac{cm}{s}$
(6) $V_{\ddot{O}} + H_2O \xrightarrow{k_6} O_O + 2H^+$	2 6		6	$\frac{cm}{s}$
(7) $MO_{t/2} + tH^+ \xrightarrow{k_7} M^{u+} + \frac{t}{2} H_2O + (u - t)e^-$	7 (-)		7(-)	$\frac{mol}{cm^2 s}$

Let us assume that the applied potential changes sinusoidally around some mean value (\bar{V}) in accordance with Equation (7):

$$V = \bar{V} + uV = \bar{V} + \Delta V e^{j\omega t} \quad (7)$$

$$k_i = k_i^0 \exp[a_i(V - R_{ol}I) - b_i L], i = 1, 2, 3 \quad (4)$$

$$k_i = k_i^0 \exp[a_i(V - R_{ol}I)], i = 4, 5 \quad (5)$$

and

$$k_7 = k_7^0 \exp[a_7(V - R_{ol}I)] \left(\frac{C_{H^+}}{C_{H^+}^0} \right)^n \quad (6)$$

where n is the kinetic order of barrier layer dissolution with respect to H^+ . In deriving these expressions theoretically, it is assumed that a resistive outer layer, R_{ol} , exists on the surface of the barrier layer and that the passive current flows through the outer layer to a remote cathode, which is the normal experimental configuration. Because of this, the potential that exists at the bl/ol interface must be corrected from that applied at the reference electrode located at the outer layer/solution interface by the potential drop across the outer layer, where R_{ol} (cm^2) is the specific resistance of the outer layer. The coefficients in the rate constant expressions are summarized in Table 1.

where ω is the angular frequency and ΔV is the amplitude. The bar over a letter refers to the corresponding value under steady-state conditions. Accordingly, in the linear approximation the independent variables have the following response

$f = \bar{f} + \Delta f e^{j\bar{S}t}$, where f represents current density, I , and values on which I depends, namely, L , C_i^0 , C_ϵ^L , and the various rate constants.

Our task, then, is to calculate the faradic admittance, Y_F , which is defined as:

$$Y_F = \frac{1}{Z_F} = \frac{uI}{uV} = \frac{\Delta I}{\Delta V} \quad (8)$$

where Z_F is the faradic impedance. Note that I , is a function of the potential at the bl/ol interface (U), but the potential that is modulated is that at the outer layer/solution (ol/s) interface (V), or close to it, depending upon the exact placement of the tip of the Luggin probe. The two potentials are related by

$$U = V - R_{ol}I \quad (9)$$

It is evident, then, that,

$$\frac{1}{Y_F} = \frac{1}{Y_F^0} + \frac{1}{R_{ol}} \text{ or } Y_F = \frac{Y_F^0}{1 + R_{ol}Y_F^0} \quad (10)$$

where Y_F^0 is the admittance calculated in the absence of the outer layer, assuming that the potential at the bl/ol interface is \bar{U} under steady-state conditions. We see that $Y_F \rightarrow Y_F^0$ as $R_{ol} \rightarrow 0$ and $Y_F \rightarrow 1/R_{ol}$ for $Y_F^0 \rightarrow \infty$; that is, the interphasial impedance becomes controlled by the outer layer in the limit of an infinitely large outer layer specific resistance or infinitely small barrier. The values of \bar{U} and other steady state values can be easily calculated. Assuming some arbitrary value of \bar{U} , we can immediately calculate \bar{k}_i , $i = 4, 5, 7$ from Equations (5) and (6). From the rate equation for the change in thickness of the barrier layer, which is written as

$$\frac{dL}{dt} = \Omega k_3 - \Omega k_7 \quad (11)$$

we have $\bar{k}_3 = \bar{k}_7$, i.e.

$$L_{ss} = \left(\frac{a_7 - a_3}{b_3} \right) U + \left(\frac{C_7 - C_3}{b_3} \right) pH + \frac{1}{b_3} \ln \left[\left(\frac{k_7^0}{k_3^0} \right) \left(\frac{C_H}{C_H^0} \right)^n \right] \quad (12)$$

After that, the values \bar{k}_i ($i = 1, 2$) can be calculated by using Equations (4).

The values of the steady-state concentrations \bar{C}_ϵ^L , \bar{C}_o^0 and \bar{C}_i^0 (concentrations of metal vacancies at the m/bl interface and of oxygen vacancies and metal interstitials at the bl/ol interface, respectively) can be found by equating

the rates of formation and annihilation at the two interfaces to yield:

$$\bar{C}_v^L = \frac{\bar{k}_4}{k_1} \quad (13)$$

$$\bar{C}_i^0 = \frac{\bar{k}_2}{k_5} \quad (14)$$

and

$$\bar{C}_o^0 = \frac{\bar{k}_3}{k_6} \quad (15)$$

Equations (13) to (15) follow from the condition that steady state fluxes of cation vacancies, cation interstitials, and oxygen vacancies, are the same at the two interfaces; otherwise time-dependent defect accumulations would occur.

Finally, we calculate the values of

$$\bar{I} = F \left\{ \begin{array}{l} t \bar{k}_1 \bar{C}_v^L + t \bar{k}_2 + t \bar{k}_3 + (u - t) \bar{k}_4 \\ + (u - t) \bar{k}_5 \bar{C}_i^0 + (u - t) \bar{k}_7 \end{array} \right\} \quad (16)$$

and

$$\bar{V} = \bar{U} + R_{ol} \bar{I} \quad (17)$$

i.e. we calculate the polarization behavior as the dependence $\bar{I}(\bar{V})$. As the actual value of \bar{U} , we will choose the value at which \bar{V} equals the prescribed value, because no outer layer is assumed in defining the impedance of the barrier layer, in this analysis. Practically, the task is reduced to the solution of the single equation $\bar{V} = \bar{U} + R_{ol} \bar{I}(\bar{U})$ relative to the unknown value \bar{U} (the voltage at the bl/ol interface).

It is important to recognize that, if we have a code for calculating the admittance of the system in the absence of the outer layer, Y_F^0 , we can derive the admittance in the presence of the outer layer, Y_F , by using Equation (10), assuming that Y_F^0 is calculated at the steady state applied potential that equals \bar{U} (but not \bar{V}).

Derivation of Y_F^0

From Equation (3) we can write, in the linear form:

$$Y_F^0 = \frac{uI}{uU} = \frac{\Delta I}{\Delta U} = I_U + I_L \frac{\Delta L}{\Delta U} + I_v^L \frac{\Delta C_v^L}{\Delta U} + I_i^0 \frac{\Delta C_i^0}{\Delta U} \quad (18)$$

where

$$I_U = F \left\{ \begin{aligned} & \tau a_1 \bar{k}_1 \bar{C}_v^L + \tau \bar{k}_2 a_2 + \tau \bar{k}_3 a_3 + (u - \tau) \bar{k}_4 a_4 \\ & + (u - \tau) \bar{k}_5 a_5 \bar{C}_i^0 + (u - \tau) \bar{k}_7 a_7 \end{aligned} \right\} \quad (19)$$

$$I_L = -F \left\{ \tau b_1 \bar{k}_1 \bar{C}_e^L + \tau \bar{k}_2 b_2 + \tau \bar{k}_3 b_3 \right\} \quad (20)$$

$$I_v^L = F \tau \bar{k}_1 \quad (21)$$

$$I_i^0 = F(u - \tau) \bar{k}_5 \quad (22)$$

Here, it is assumed that the imposed voltage varies sinusoidally, $U = \bar{U} + uU = \bar{U} + \Delta U e^{j\tilde{S}t}$ and the four terms on the right side can be attributed to relaxations with respect to the applied potential V , the thickness of the barrier layer with respect to the voltage at the bl/ol interface, U , cation vacancies, \bar{C}_v^L , and cation interstitials, \bar{C}_i^0 , respectively. Note the absence of a term for the relaxation of oxygen vacancies, because, again, the concentration of oxygen vacancies does not appear in the current [Equation (3)], because of assuming that Reaction (3), Figure 1, is irreversible. Physically, though, the oxygen vacancies carry at least part of the current, so that the concomitant transport impedance must be accounted for. This is done by adding a Warburg impedance (Z_W) element in series with the Faradaic impedance (Z_F) as explained later in the paper. Thus, the Faradaic impedance is redefined as being $Z_F + Z_W$.

Let us now derive expressions for $\frac{\Delta L}{\Delta U}$, $\frac{\Delta C_v^L}{\Delta U}$ and $\frac{\Delta C_i^0}{\Delta U}$. For reasons that will become

apparent below, it is convenient to start with $\frac{\Delta L}{\Delta U}$.

The rate of change of the thickness of the barrier layer is described by Equation (11). Thus, by taking the total differential of Equation (11), we obtain

$$\frac{duL}{dt} = j\tilde{S}\Delta L e^{j\tilde{S}t} = \Omega u k_3 - \Omega u k_7 = \quad (23)$$

$$\Omega(\bar{k}_3 a_3 u U - \bar{k}_3 b_3 u L) - \Omega \bar{k}_7 a_7 u V$$

or

$$L_U \equiv \frac{\Delta L}{\Delta U} = \frac{\Omega(\bar{k}_3 a_3 - \bar{k}_7 a_7)}{j\tilde{S} + \Omega \bar{k}_3 b_3} \quad (24)$$

which is the desired result.

Derivation of $\Delta C_i^0 / \Delta U$

The flux density of interstitials is

$$J_i = -D_i \frac{\partial C_i}{\partial x} - \tau D_i K C_i \quad (25)$$

In this expression, D_i is the diffusion coefficient of the cation interstitials, $K = F/RT$, where F is the electric field strength of the barrier layer, and T is the temperature. The continuity equation is then written as:

$$\frac{\partial C_i}{\partial t} = D_i \frac{\partial^2 C_i}{\partial x^2} + \tau D_i K \frac{\partial C_i}{\partial x} \quad (26)$$

which must be solved subject to the boundary conditions

$$-k_5 C_i = -D_i \frac{\partial C_i}{\partial x} - \tau D_i K C_i \text{ at } x = 0 \quad (27)$$

Substitution $C_i = \bar{C}_i + \Delta C_i e^{j\tilde{S}t}$ into Equations (25) to (27) and linearization of the boundary conditions relative to U and L yields:

$$j\tilde{S}U C_i = \frac{\partial^2 U C_i}{\partial x^2} + \tau D_i K \frac{\partial U C_i}{\partial x} \quad (28)$$

or

$$-\bar{k}_5(\bar{C}_i^0 a_5 \Delta U + \Delta \bar{C}_i^0) = -D_i \left(\frac{\partial \Delta C_i}{\partial x} \right)_{x=0} \quad (29)$$

$$- \tau D_i K \Delta C_i^0 \text{ at } x = 0$$

$$-\bar{k}_2(a_2 \Delta U - b_2 \Delta L) = -D_i \left(\frac{\partial \Delta C_i}{\partial x} \right)_{x=L} \quad (30)$$

$$- \tau D_i K \Delta C_i^L \text{ at } x = L$$

Analytical solution of the linear boundary problem (28) – (30) is easily obtained and the sought value $\Delta C_i^0 / \Delta U$ can be presented in the following form:

$$\frac{U C_i^0}{U U} = \frac{A + B}{U U} = U C_{iU}^0 + U C_{iL}^0 \frac{U L}{U U} \quad (31)$$

where

$$\Delta C_{iU}^0 = \frac{b_{1U}(a_{22} - a_{21}) + b_{2U}(a_{11} - a_{12})}{a_{11}a_{22} - a_{12}a_{21}} \quad (32)$$

$$\Delta C_{iL}^0 = \frac{b_{2L}(a_{11} - a_{12})}{a_{11}a_{22} - a_{12}a_{21}} \quad (33)$$

$$r_{1,2} = \frac{-\tau K \pm \sqrt{\tau^2 K^2 + 4j\tilde{S}/D_i}}{2} \quad (34)$$

$$a_{11} = (r_1 + \tau K)D_i - \bar{k}_5, \quad a_{12} = (r_2 + \tau K)D_i - \bar{k}_5, \quad (35)$$

$$a_{21} = (r_1 + \tau K)D_i e^{r_1 L}, \quad a_{22} = (r_2 + \tau K)D_i e^{r_2 L}$$

$$b_{1U} = \bar{k}_5 a_5 \bar{C}_i^0, \quad b_{2U} = \bar{k}_2 a_2, \quad b_{2L} = -\bar{k}_2 b_2 \quad (36)$$

and $\frac{UL}{UU}$ is given by Equation (24).

The reader should note that the expressions given above for cation interstitials can be shown to be the same as those for oxygen vacancies, with the oxidation number, t , being replaced by 2, Subscript 2 being replaced by Subscript 3, and Subscript 5 being replaced by Subscript 6, so as to identify the correct reactions in Figure 1.

Derivation of $\Delta C_v^L / \Delta U$

By analogy with the above it can be shown that:

$$\frac{\Delta C_\epsilon^L}{\Delta U} = \frac{Ae^{\eta^L} + Be^{r_2^L}}{\Delta U} = \Delta C_{vV}^L + \Delta C_{vL}^L \frac{\Delta L}{\Delta U} \quad (37)$$

where

$$\Delta C_{vV}^L = \frac{(b_{1U}a_{22} - b_{2U}a_{12})e^{\eta^L} + (b_{2U}a_{11} - b_{1U}a_{21})e^{r_2^L}}{a_{11}a_{22} - a_{12}a_{21}} \quad (38)$$

$$\Delta C_{vL}^L = \frac{b_{2L}a_{11}e^{r_2^L} - b_{2L}a_{12}e^{\eta^L}}{a_{11}a_{22} - a_{12}a_{21}} \quad (39)$$

$$r_{1,2} = \frac{tK \pm \sqrt{t^2 K^2 + 4j\bar{S}/D_v}}{2} \quad (40)$$

where

$$\begin{aligned} a_{11} &= (r_1 - tK)D_v, & a_{12} &= (r_2 - tK)D_v, \\ a_{21} &= [(r_1 - tK)D_v + \bar{k}_1]e^{\eta^L}, & & \\ a_{22} &= [(r_2 - tK)D_v + \bar{k}_1]e^{r_2^L} \end{aligned} \quad (41)$$

$$\begin{aligned} b_{1U} &= -\bar{k}_4 a_4, \\ b_{2U} &= -\bar{k}_1 a_1 \bar{C}_v^L, \\ b_{2L} &= \bar{k}_1 \bar{C}_v^L b_1 \end{aligned} \quad (42)$$

and, again, $\frac{UL}{UU}$ is given by Equation (24).

By substituting Equations (24), (31) and Equation (37) into Equation (18) we have the result:

$$Y_F^0 = I_U + I_L L_U + I_v^L (\Delta C_{vU}^L + \Delta C_{vL}^L L_U) + I_i^0 (\Delta C_{iU}^0 + \Delta C_{iL}^0 L_U) \quad (43)$$

The Swedish plan for the isolation of high-level nuclear waste (HLNW) calls for encapsulation of spent nuclear fuel in a copper canister located within bore holes within a crystalline bedrock repository at a depth of about 500 m. The groundwater is a brine containing bi-sulfide ion (HS^-), which is known to activate the corrosion of

copper [21]. The current plan calls for emplacement of spent fuel in an inner cast iron canister shielded with a 50 mm thick outer layer of metallic copper [22–24], which, in turn, is surrounded by a layer of compacted bentonite. After emplacement of the canisters in the boreholes in the floors of the drifts (tunnels), the remaining space will be backfilled with a compacted bentonite clay buffer [22]. The role of the inner cast iron layer is to provide mechanical strength as well as radiation shielding, while the copper outer layer provides corrosion protection. Hydration of the bentonite layer produces a highly impervious barrier to the transport of deleterious species, such as HS^- , to the copper surface, representing one barrier in the multi-barrier concept for HLNW disposal. Thus, in the anoxic groundwater environment, corrosion mechanisms involving sulfides have been identified by SKB (the Swedish vendor of the disposal technology) to be important in controlling canister lifetime [24]. Sulfide species, such as bisulfide ion (HS^-), are present in groundwater in the near-field environment and hence in the vicinity of the copper canisters. As noted above, these species are powerful activators of copper corrosion [21] by inducing a partial anodic reaction ($2Cu + HS^- \rightarrow Cu_2S + H^+ + 2e^-$) at a potential that is about 600 mV more negative than that for the formation of the oxide ($2Cu + H_2O \rightarrow Cu_2O + 2H^+ + 2e^-$) in the absence of sulfide. Thus, in the presence of sulfide species, copper is converted from being a semi-noble metal to an active metal [21], resulting in corrosion and hence in a reduction of the canister lifetime.

Figure 2 displays the potentiodynamic polarization curves of copper in a deaerated 0.1 M $NaCl + 2 \times 10^{-4}$ M $Na_2S \cdot 9H_2O$ solution at 25 °C, as measured in our previous work [25,26].

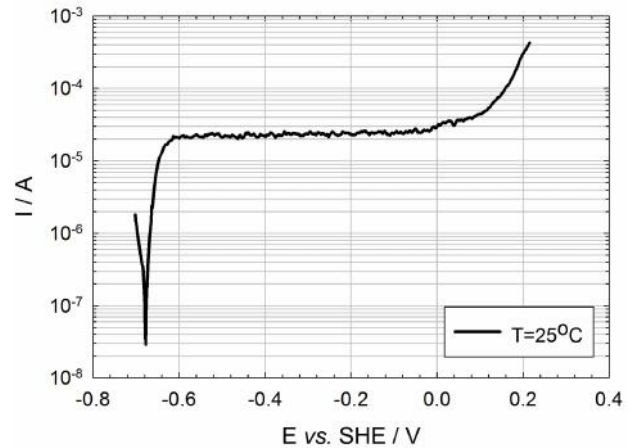


Fig. 2. Potentiodynamic polarization curves of Cu in a deaerated 0.1 M $NaCl + 2 \times 10^{-4}$ M $Na_2S \cdot 9H_2O$ solution at 25 °C. (Scan rate = 1 mV s⁻¹).

A broad passive range of potential is observed, starting from about -0.7 (potential which is related to the formation of copper sulfide) and extending up to +0.15 V vs. SHE. Four potentials within the passive region were selected for the impedance analysis, -0.495 V, -0.395 V, -0.295 V and -0.195 V vs. SHE, with the electrode at these potentials being controlled potentiostatically for the entire time of the experiments.

A modified point defect model (PDM) for the formation of the bi-layer $Cu/Cu_2S/CuS$ passive films on copper in the sulfide-containing solutions was proposed [26]. The physico-chemical basis of the modified PDM is shown in Figure 3. In this study, we propose a PDM specifically for the growth and dissolution of the passive sulfide films on copper.

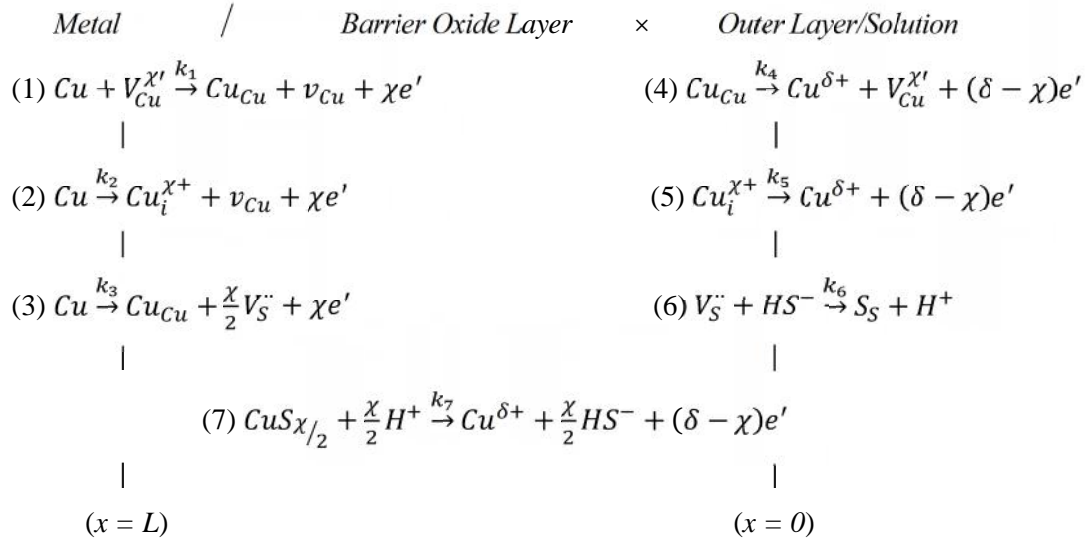


Fig. 3. Interfacial defect generation/annihilation reactions that are postulated to occur in the growth of anodic barrier sulfide films ($χ = 1$ for both Cu_2S and CuS , where the latter is the Cu(I) salt of the disulfide ion, S_2^{2-}) according to the Point Defect Model. $V_{Cu}^{χ'}$ ≡ cation vacancy on the metal sublattice of the barrier layer, $Cu_i^{χ+}$ ≡ cuprous cation interstitial, Cu_{Cu} ≡ cuprous cation in cation site on the metal sublattice of the Cu_2S barrier layer $V_S^{..}$ ≡ sulfur vacancy on the anion sublattice of the barrier layer, S_S ≡ sulfur anion on the anion sublattice of the barrier layer, Cu^{u+} ≡ cuprous cation in solution.

Note that the model is written in general form; being capable of describing the formation of both Cu_2S and CuS barrier layers.

Figures 4 and 5 display typical experimental electrochemical impedance spectra (Nyquist and Bode plots) for the passive sulfide film formed on copper in a deaerated 0.1 M $NaCl + 2 \times 10^{-4}$ M $Na_2S \cdot 9H_2O$ solution at 25°C. The best fit results, calculated from the parameters obtained from optimization of the proposed mechanism (Figure 3) on the experimental EIS data are listed in Tables 2 and 3, and the impedance calculated from those parameters are also included in Figures 4 and 5 as solid lines. One will note that the correlation between experiment and the model is very good, indicating that the proposed model (Figure 3) provides an excellent account of the observed experimental data.

Table 2. Averaged Kinetic parameters obtained from the PDM optimization of copper in a deaerated 0.1 M $NaCl + 2 \times 10^{-4}$ M $Na_2S \cdot 9H_2O$, at 25°C.

Parameter	Value	Dimensions
	0.26	-
1	0.44	-
3	0.21	-
4	0.07	-
n	-0.15	-
k ₁	3.52×10^{-07}	(s ⁻¹)
k ₂	1.85×10^{-16}	(mol cm ² s ⁻¹)
k ₃	2.46×10^{-11}	(mol cm ² s ⁻¹)
k ₄	7.85×10^{-13}	(mol cm ² s ⁻¹)
k ₇	7.31×10^{-13}	(mol cm ² s ⁻¹)

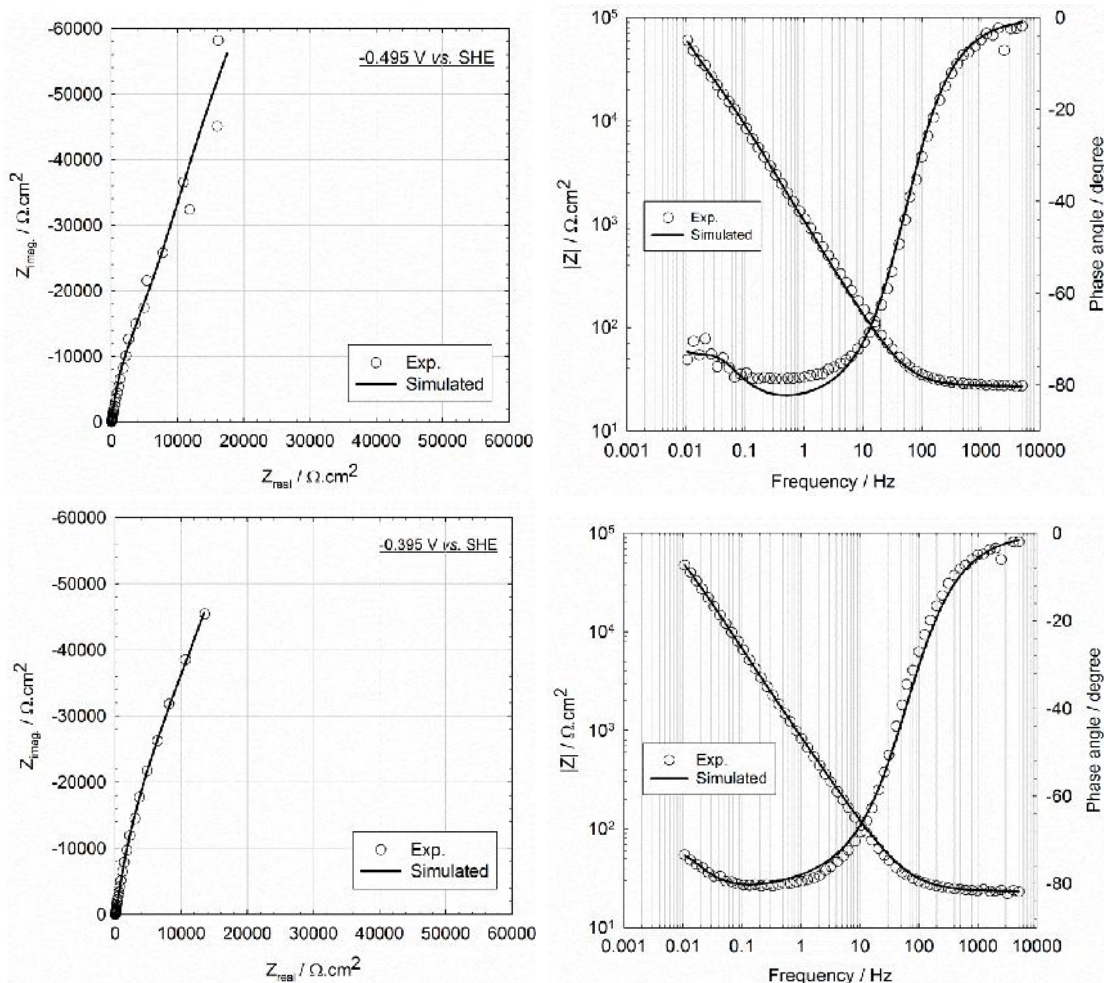


Fig. 4. Experimental and simulated Nyquist and Bode plots for copper in a deaerated 0.1 M NaCl + 2×10^{-4} M $Na_2S.9H_2O$, $T = 25^\circ C$ as a function of applied potential, solid lines show the best fit calculation of the PDM using the optimized parameter values

It is important to note that the obtained parameters should not only reproduce the experimental impedance spectra, but should also deliver values of various properties that are physically reasonable. Thus, the obtained kinetic parameters, such as the standard rate constants, transfer coefficients, and defect diffusivities listed in Tables 2 and 3, show no systematic dependency on the applied potential as required by the fundamental electrochemical kinetic theory. This is a good test of viability of the proposed model. Of particular interest is the value of the electric field strength as a function of voltage. It is seen that the value (2.1×10^5 V/cm) is about an order of magnitude lower than that typically found for oxide barrier layers [14], corresponding with the greater polarizability of the sulfide compared with the oxide ion. Furthermore, within experimental accuracy, the electric field strength is independent of the applied voltage, confirming one of the important postulates upon which the PDM is based.

Cuprous sulfide, Cu_2S , is a p-type semiconductor, indicating that the dominant point defect

in the lattice is the cation vacancy. The value of the cation vacancy diffusivity is quite high [$(1.0 \pm 0.7) \times 10^{-13}$ cm^2/s] and appears to display some voltage-dependence, although the experimental uncertainty is difficult to judge accurately. Also, the diffusivity is a “deeply buried” parameter in the model, so that its value is possibly only semi-quantitative in nature. Nevertheless, it is in reasonably good agreement with the value of 10^{-15} to 10^{-14} cm^2/s that is predicted theoretically using Density Functional Theory (DFT) [27]. As mentioned in the previous section, the rate of change of the barrier layer thickness that forms on a metal surface can be expressed as:

$$\frac{dL}{dt} = k_3^0 e^{a_3 V} e^{b_3 L} e^{c_3 p H} - k_7^0 \left(\frac{C_{H^+}}{C_{H^+}^0} \right)^n e^{a_7 V} e^{c_7 p H} \quad (44)$$

where Ω is the molar volume of the barrier layer per cation, C_{H^+} is the concentration of hydrogen ion, $C_{H^+}^0$ is the standard state concentration, and “ n ” is the kinetic order of the barrier layer dissolution reaction with respect to H^+ .

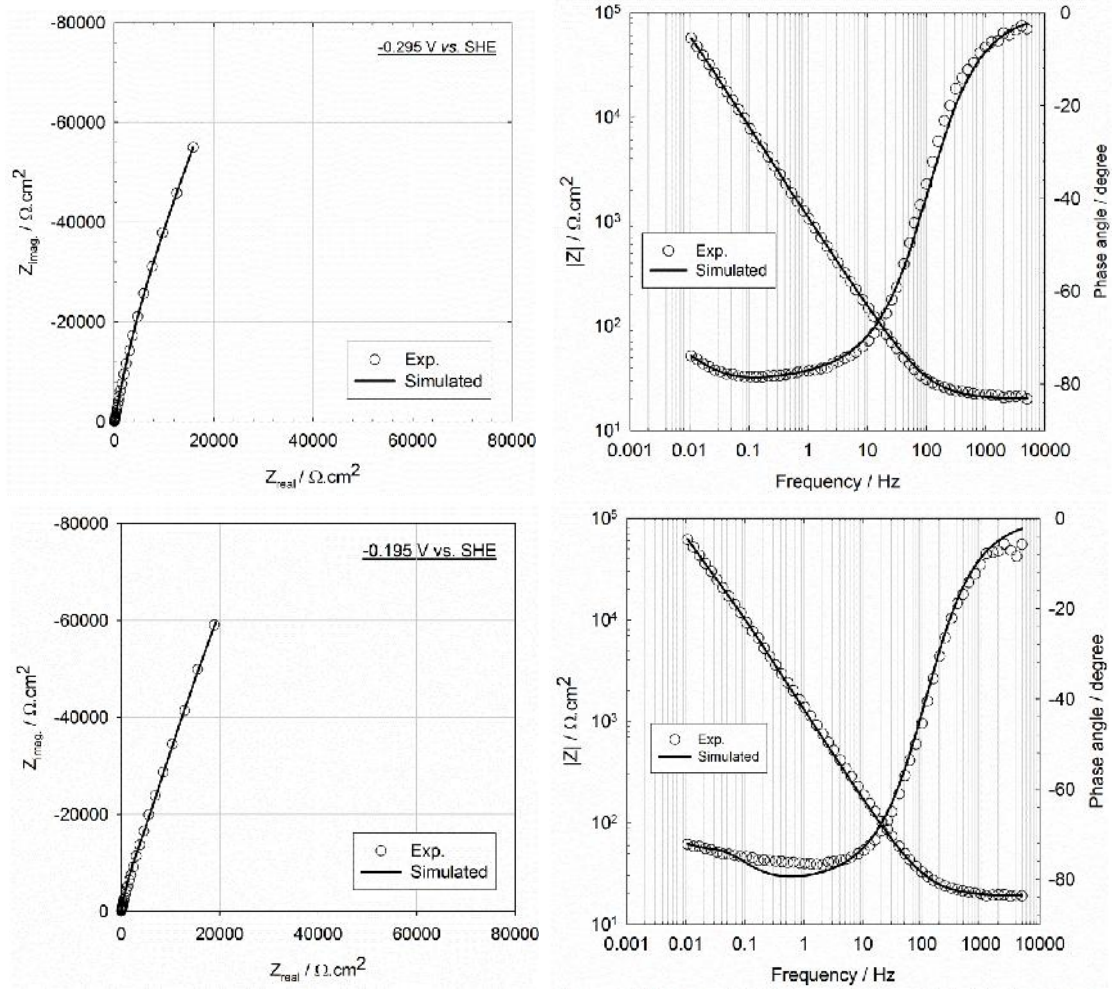


Fig. 5. Experimental and simulated Nyquist and Bode plots for copper in a deaerated 0.1 M NaCl + 2×10^{-4} M $Na_2S \cdot 9H_2O$, $T = 25^\circ C$ as a function of applied potential, solid lines show the best fit calculation of the PDM using the optimized parameter values

Definitions of the other parameters are listed in Table 2. It should be mentioned that, since the pH of the solution was higher than the pH of zero charge for Cu_2S and CuS dissolution ($PZC < 3.5$ [28]), “ n ” should be a negative value as is obtained from the optimization. Another point to be noted is that the rate of the dissolution reaction is potential dependent if the oxidation state of copper in the barrier layer is different from its oxidation state in the solution. However, under an anoxic condition, the oxidation state of copper in both phases is +1, in that CuS is the $Cu(I)$ salt of the disulfide (S_2^{2-}) and should be written as Cu_2S_2 . Therefore, the rate of film dissolution is considered to be potential-independent.

Under steady-state conditions $\frac{dL}{dt} = 0$ and the steady-state thickness of the barrier layer can be derived as:

$$L_{SS} = \left[\frac{1-\alpha}{\varepsilon} \right] V + \left[\frac{2.303n}{\alpha_3 \varepsilon_{XY}} - \frac{\beta}{\varepsilon} \right] pH + \frac{1}{\alpha_3 \varepsilon_{XY}} \ln \left(\frac{k_3^0}{k_7^0} \right) \quad (45)$$

Figure 6(a) shows a comparison of the calculated steady-state thickness of the barrier layer with the experimental results as a function of applied potential, while the steady-state current for passive copper in sulfide-containing sodium chloride solution calculated from the parameters obtained from the PDM optimization is shown in Figures 6(b). As seen from these figures, there is a linear dependence of $\log(I_{ss})$ on the applied potential, which is consistent with the PDM diagnostic criteria for p-type passive films. The parameters obtained from the PDM optimization listed in Tables 2 and 3 were used to calculate theoretically the steady-state properties (thickness and passive current density) of the barrier layer using Equations.16 and 45.

Table 3. Other parameters obtained from the Simulation of the proposed model for copper in a deaerated 0.1 M NaCl+2×10⁻⁴ M Na₂S.9H₂O, at 25°C .

E _{app.} (V vs. SHE)	-0.495	-0.395	-0.295	-0.195	Origin
	1	1	1	1	Assumed
	1	1	1	1	Assumed
CPE-g (S s cm ⁻²)	5.31×10 ⁻⁰⁴	4.90×10 ⁻⁰⁴	2.93×10 ⁻⁰⁴	2.71×10 ⁻⁰⁴	2 nd stage optim
CPE-	0.82	0.78	0.81	0.83	2 nd stage optim
pH	10.18	10.18	10.18	10.18	Measured
(V cm ⁻¹)	1.94×10 ⁺⁰⁵	2.10×10 ⁺⁰⁵	2.10×10 ⁺⁰⁵	2.20×10 ⁺⁰⁵	1 st stage optim
C _{dl} (F cm ⁻²)	1.60×10 ⁻⁰⁴	2.22×10 ⁻⁰⁴	1.43×10 ⁻⁰⁴	1.38×10 ⁻⁰⁴	2 nd stage optim
R _{ct} (cm ²)	2.80×10 ⁺⁰⁵	9.99×10 ⁺¹⁰	9.98×10 ⁺¹⁰	9.99×10 ⁺¹⁰	2 nd stage optim
R _s (cm ²)	27	23	19	18	Estimated
D _v (cm ² s ⁻¹)	7.44×10 ⁻¹⁴	1.00×10 ⁻¹³	1.00×10 ⁻¹³	7.45×10 ⁻¹³	2 nd stage optim
R _{ol} (cm ²)	4.27×10 ⁺⁰⁴	1.03×10 ⁺⁰⁵	1.48×10 ⁺⁰⁵	2.78×10 ⁺⁰⁴	2 nd stage optim
C _{ol} (F cm ⁻²)	2.35×10 ⁻⁰⁴	4.01×10 ⁻⁰⁴	4.66×10 ⁻⁰⁴	3.04×10 ⁻⁰⁴	2 nd stage optim
(cm ² s ^{-0.5})	10	10	11	12	2 nd stage optim
R _{e,h} (cm ²)	9.11×10 ⁺¹⁰	9.94×10 ⁺¹⁰	1.00×10 ⁺⁰⁷	1.00×10 ⁺⁰⁷	2 nd stage optim
L _{SS} (cm)	3.86×10 ⁻⁰⁷	7.65×10 ⁻⁰⁷	1.14×10 ⁻⁰⁶	1.42×10 ⁻⁰⁶	Calculated
I _{SS} (A cm ⁻²)	2.43×10 ⁻⁰⁶	2.44×10 ⁻⁰⁶	2.45×10 ⁻⁰⁶	2.46×10 ⁻⁰⁶	Calculated

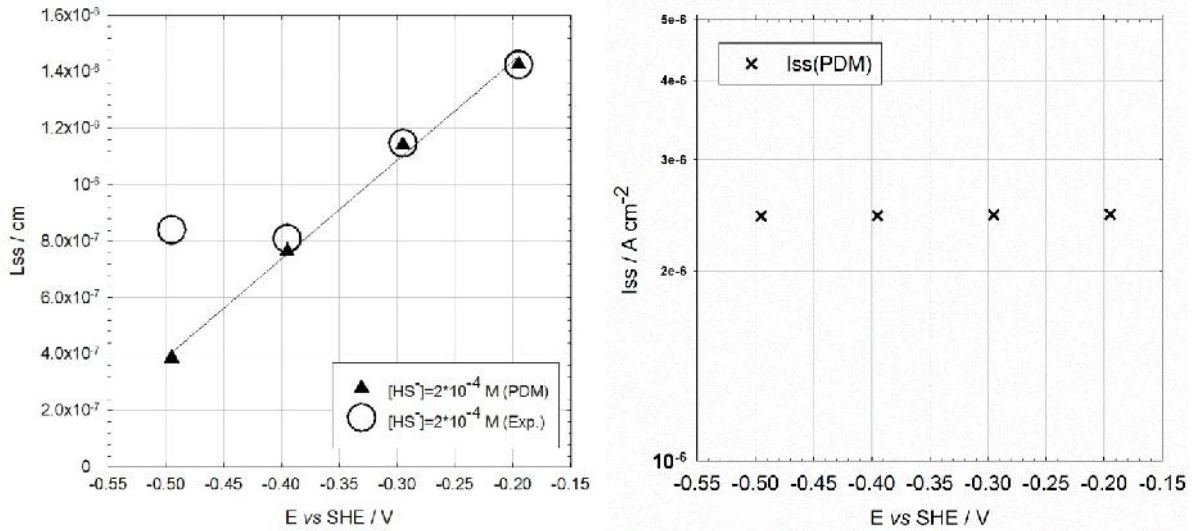


Fig. 6. Plots of the calculated and experimental steady-state barrier layer thickness as a function of potentials for copper in a deaerated 0.1 M NaCl+2×10⁻⁴ M Na₂S.9H₂O at 25°C.

In order to obtain the experimental steady-state thickness, we used the well-known parallel plate capacitance formula (Eq.46) assuming a value of the capacitance from the high frequency (1 kHz) imaginary part of the experimental impedance data.

$$C = \frac{\tilde{\epsilon}\epsilon^0}{d} \quad (46)$$

where $\tilde{\epsilon}$ is the dielectric constant (calibrated based on the obtained thickness, $\tilde{\epsilon} = 724$), $\epsilon^0 = 8.85 \times 10^{-14}$ (F cm⁻¹) is the vacuum permittivity, d is the thickness of the film (cm), and C is the capacitance (F cm⁻²). As can be seen, the thickness of the barrier layer increases with applied potential as predicted by the PDM [1-5]. Good agreement is obtained

between the calculated and experimental thickness except at the lowest potential, which is closest to the active-to-passive transition (Fig. 2) and it is possible that the barrier layer had not fully developed at that potential. This postulate is somewhat supported by the fact that instabilities were observed in the impedance measurements at that potential.

SUMMARY AND CONCLUSIONS

In this paper, we illustrate the application of electrochemical impedance spectroscopy (EIS) in analyzing impedance data for passive metal systems. We demonstrate the feasibility of deriving an impedance version of the Point Defect Model (PDM) and of optimizing the model upon experimental impedance data to extract values for important model parameters. These, in turn, are used to calculate the steady state barrier layer thickness and passive current density as a function of voltage. This work provides a scientific basis for estimating the lifetimes of copper canisters in crystalline rock repositories in Sweden for the disposal of high level nuclear waste (HLNW).

Acknowledgements: *The authors gratefully acknowledge the support of this work by Strålsäkerhets myndigheten (SSM) of Sweden.*

REFERENCES

1. C. Y. Chao, L. F. Lin, and D. D. Macdonald, "A Point Defect Model for Anodic Passive Films I. Film Growth Kinetics," *J. Electrochem. Soc.*, **128**, 1187 (1981).
2. L. F. Lin, C. Y. Chao, and D. D. Macdonald, "A point defect model for anodic passive films II. Chemical breakdown and pit initiation," *J. Electrochem. Soc.*, **128**, 1194 (1981).
3. C. Y. Chao, L. F. Lin, D. D. Macdonald, "A Point Defect Model for Anodic Passive Films III. Impedance Response," *J. Electrochem. Soc.*, **129**, 1874–1879 (1982).
4. D. D. Macdonald, "Passivity-the key to our metals-based civilization," *Pure Appl. Chem.*, **71**, 951 (1999).
5. D. D. Macdonald, "On the Existence of Our Metals-Based Civilization," *J. Electrochem. Soc.*, **153**, B213 (2006).
6. H. Song, D. D. Macdonald, "Photoelectrochemical Impedance Spectroscopy I. Validation of the Transfer Function by Kramers-Kronig Transformation," *J. Electrochem. Soc.*, **138**, 1408 (1991).
7. D. D. Macdonald, E. Sikora, M. W. Balmas, R. C. Alkire, "The photo-inhibition of localized corrosion on stainless steel in neutral chloride solution," *Corros. Sci.*, **38**, 97 (1996).
8. M. Urquidi, D. D. Macdonald, "Solute-Vacancy Interaction Model and the Effect of Minor Alloying Elements on the Initiation of Pitting Corrosion," *J. Electrochem. Soc.*, **132**, 555 (1985).
9. L. Zhang, D. D. Macdonald, "Segregation of alloying elements in passive systems—I. XPS studies on the Ni–W system," *Electrochim. acta*, **43**, 2661 (1998).
10. D. D. Macdonald and S. I. Smedley, "An electrochemical impedance analysis of passive films on nickel (111) in phosphate buffer solutions," *Electrochim. Acta*, **35**, 1949 (1990).
11. D. D. Macdonald, M. Urquidi-Macdonald, "Application of Kramers-Kronig Transforms in the Analysis of Electrochemical Systems I. Polarization Resistance," *J. Electrochem. Soc.*, **132**, 2316 (1985).
12. M. Urquidi-Macdonald, S. Real, and D. D. Macdonald, "Application of Kramers-Kronig Transforms in the Analysis of Electrochemical Impedance Data II. Transformations in the Complex Plane," *J. Electrochem. Soc.*, **133**, 2018 (1986).
13. J. Ai, Y. Chen, M. Urquidi-Macdonald, D. D. Macdonald, "Electrochemical Impedance Spectroscopic Study of Passive Zirconium," *J. Electrochem. Soc.*, **154**, C52 (2007).
14. D. D. Macdonald, A. Sun, "An electrochemical impedance spectroscopic study of the passive state on Alloy-22," *Electrochim. Acta*, **51**, 1767 (2006).
15. J. Geringer, M. L. Taylor, D. D. Macdonald, "Predicting the steady state thickness of passive films with the point defect model in fretting corrosion experiments," Proceedings of PRIME 2012 (22nd Electrochemical Society Meeting, Pacific Rim Meeting on Electrochemical and Solid State Science), 2012.
16. DataFit, Oakdale Engineering, www.oakdaleengr.com.
17. K. Levenberg, "A method for the solution of certain problems in least squares", *The Quart. Appl. Math.*, **2**, 164 (1944).
18. "Ellis 2: Complex curve fitting for one independent variable | IgorExchange.", 2012.
19. T. Bäck, H.-P. Schwefel, "An Overview of Evolutionary Algorithms for Parameter Optimization," *Evolutionary computation*, **1**, 1 (1993).
20. [D. D. Macdonald, and G. R. Engelhardt, "The Point Defect Model for Bi-Layer Passive Films", *ECS Trans*, **28**(24), 123 (2010).
21. S. Sharifi-Asl and D. D. Macdonald. "Corrosion domain analysis of copper corrosion in aqueous media", *Corr. Eng. Sci. Tech.*, **50**, 467-470 (2015).
22. F. King, L. Ahonen, C. Taxén, U. Vuorinen, and L. Werme, "Copper corrosion under expected conditions in a deep geologic repository," Swedish Nuclear Fuel and Waste Management Company Report, SKB TR 01-23, 2001 and Posiva Oy Report POSIVA 2002-01, 2002.
23. F. King, "Container Materials for the Storage and Disposal of Nuclear Waste," *Corrosion*, **69**, 986 (2013).
24. King, C. Lilja, M. Vähänen, "Progress in the understanding of the long-term corrosion behaviour of copper canisters," *Journal of Nuclear Materials*, **438**, 228 (2013).

25. S. Sharifi-Asl, "Corrosion issues in high-level nuclear waste containers", Diss. The Pennsylvania State University, 2013.
26. C-F. Dong, F. Mao, S. Gao, S. Sharifi-Asl, P. Lu, D. D. Macdonald, Passivity Breakdown on Copper: Influence of Temperature, *Journal of The Electrochemical Society*, **163(13)**, C707 (2016).
27. M. Kosmulski, Surface charging and points of zero charge, Surfactant Science Series, Vol. **145**, CRC Press, Boca Raton, FL 2010, p. 1696.